Double-pass acousto-optic modulator system

E. A. Donley,[a] T. P. Heavner, F. Levi,[b] M. O. Tataw, and S. R. Jefferts
Time and Frequency Division, National Institute of Standards and Technology, 325 Broadway, Boulder, Colorado 80305

(Received 2 March 2005; accepted 21 April 2005; published online 1 June 2005)

A practical problem that arises when using acousto-optic modulators (AOMs) to scan the laser frequency is the dependence of the beam diffraction angle on the modulation frequency. Alignment problems with AOM-modulated laser beams can be effectively eliminated by using the AOM in the double-pass configuration, which compensates for beam deflections. On a second pass through the AOM, the beam with its polarization rotated by 90° is deflected back such that it counterpropagates the incident laser beam and it can be separated from the input beam with a polarizing beam splitter. Here we present our design for a compact, stable, double-pass AOM with 75% double-pass diffraction efficiency and a tuning bandwidth of 68 MHz full width at half maximum for light transmitted through a single-mode fiber. The overall efficiency of the system (defined as the optical power out of the single-mode fiber divided by the optical power into the apparatus) is 60%.
[DOI: 10.1063/1.1930095]

I. INTRODUCTION

For many laser cooling and trapping experiments, it is necessary to shift and/or sweep the laser frequency at the end of a cooling cycle. This is done to either adiabatically cool the atoms to a lower temperature, or to manipulate them in some other way, such as launching them in an atomic fountain. Most often, the laser frequency must be switched on time scales shorter than 1 ms, and it may be that laser beams with several different frequencies must be produced from a single laser source.

Acousto-optic modulators (AOMs) are widely used to accomplish the frequency control in laser cooling experiments. When the laser frequency is scanned with an AOM, the angle of the first-order diffracted beam shifts as well, since the beam diffraction angle is a function of modulation frequency. Changes in beam diffraction angle may be desirable for some applications where spatially resolved diffracted beams are needed, but for many applications any change in the laser propagation direction is an unwanted side effect. Using an AOM in the double-pass configuration is a way to practically eliminate changes in beam steering during frequency sweeps and jumps within the frequency tuning bandwidth of the AOM. Here we present a detailed description of our modular double-pass system design and a study of the system's performance.

The article is organized as follows. In Sec. II, the laser frequency jump and ramp sequence that is used to cool and launch the atoms in the primary frequency standard at the National Institute of Standards and Technology (NIST) is presented in detail. This provides a real-world example of the level of laser frequency control that can be desirable for atomic physics experiments. In Sec. III, background into the properties of acousto-optic modulators is presented. In Sec. IV, the double-pass configuration is introduced, our specific design is discussed in detail, and the performance of our design is presented.

II. ATOMIC FOUNTAIN LASER FREQUENCY CONTROL

For laser cooling and trapping experiments, the optimum laser intensity and detuning values that maximize the number of laser-cooled atoms are not the same as the optimum values for the lowest atom temperature. The laser intensity that maximizes the number of atoms can depend on the details of the atom source, but in general, a higher laser intensity is better for a thermal source. The optimum laser detuning is generally a few linewidths, but it can also depend on the details of the atom source and the laser intensity. In contrast, at low laser intensities the equilibrium atom temperature in an optical molasses is equal to a small constant term ($\sim 1\ \mu$K for ^{133}Cs) plus a term that is proportional to the laser intensity and inversely proportional to the laser detuning.[1,2] To simultaneously maximize the atom number and minimize the atom temperature, often a brief "postcool" stage is applied as the molasses is turned off. During the postcool stage, the laser frequency is ramped further to the red of the atomic resonance while the intensity is ramped to zero.

The atom launch and postcool sequence for the vertical laser beams used in the NIST-F1 atomic fountain clock at NIST is shown in Fig. 1. NIST-F1 serves as the primary frequency standard for the United States, and a detailed description of the apparatus has been published previously.[3] We accomplish the frequency sweeps and jumps shown in Fig. 1 with AOMs. The intensity ramp is produced by controlling the rf power into the AOM with a voltage-controlled attenuator. With this sequence, we are able to collect about 10^7

[a]Author to whom correspondence should be addressed; electronic mail: edonley@boulder.nist.gov
[b]Permanent address: Istituto Elettrotecnico Nazionale "G. Ferraris" Str. Delle Cacce 91, Torino, Italy.

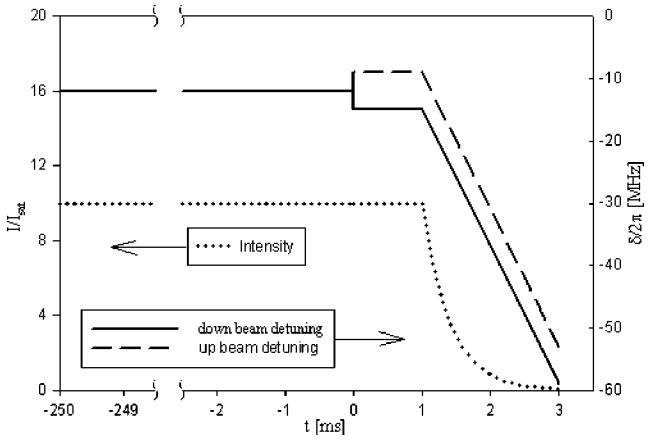

FIG. 1. Laser frequency and intensity ramps typically used for NIST-F1. The intensity is shown on the left vertical scale in units of the saturation intensity, I_{sat}. The laser detuning from resonance is indicated on the right vertical scale. The atoms are initially collected in an optical molasses for ~250 ms. To launch the atoms in a moving molasses, the frequencies of the up (down) beams are shifted from their initial frequencies by typically +2.5 MHz (−2.5 MHz) for 1 ms. Then the atoms are postcooled in the moving frame for 2 ms by ramping down the laser intensity while linearly shifting the frequencies of both beams further to the red by 44 MHz. Note that the frequency and intensity curves for the horizontal molasses beams are not shown. Those beams also have a postcool sequence, but there is no frequency step when the atoms are launched.

atoms per cycle, cool them to ~0.5 μK, and launch them into a microwave cavity structure for Ramsey interrogation.

III. ACOUSTO-OPTIC MODULATORS

A. Bragg scattering

For most practical applications of acousto-optic modulators, the Bragg description of the modulation process is a good approximation to the behavior of the system.[4,5] The main features of AOMs are derived in this picture by treating the modulation as a photon-phonon scattering process.

The Bragg matching condition can be derived by treating the acoustic and optical fields as particles with momentum κ and k, respectively, where κ (k) is the phonon (photon) wave vector for the acoustic (optical) field; $\kappa=\Omega/v_s$, where Ω is the rf modulation frequency and v_s is the speed of sound in the crystal. Similarly, $k=\omega/v_L$, where ω is the light frequency and v_L is the speed of light in the crystal.

A scattering process between photons and phonons results in the absorption or emission of acoustic phonons. A first-order scattering process between a photon and a single phonon is described by the energy-momentum relations

$$\omega_d = \omega_i \pm \Omega,$$

$$k_d = k_i \pm \kappa. \tag{1}$$

The subscripts i and d designate whether the corresponding photon is incident or diffracted. The sign depends on whether the phonon is absorbed or emitted, which depends on the relative orientations of the incident photon and phonon wave vectors.

The Bragg matching condition that determines the optimum angles for the incident laser and acoustic beams for peak first-order diffraction efficiency can be derived with energy and momentum conservation arguments. Figure 2 shows momentum conservation diagrams that describe photon-phonon scattering events in which a phonon is absorbed (+first-order diffraction). The photon momentum of the diffracted light is equal to the sum of the momenta of the phonon and the incident photon. Conservation of energy requires that the frequency of the diffracted beam be shifted upward from ω to $\omega+\Omega$ for a phonon absorption process; but since $\omega \gg \Omega$, the frequency shift can be ignored in the momentum conservation analysis, and $|k_i|=|k_d|$. Adding together the x and y momentum components leads one to Bragg's law

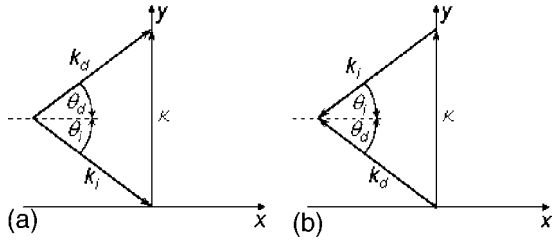

FIG. 2. Momentum conservation diagrams for the absorption of a phonon. The two cases [(a) and (b)] represent two configurations for the incident and diffracted light beams where the conditions are Bragg matched for a given orientation of the phonon momentum. Note that κ, and thus θ_i and θ_d, are made large in the diagrams for clarity. The Bragg angle is normally about 1° or less, and the phonon momentum is roughly two orders of magnitude smaller than the photon momentum.

$$\sin\theta_B = \frac{\kappa}{2\cdot k_i}, \tag{2}$$

where θ_B is the Bragg angle, and $\theta_i=\theta_d=\theta_B$. Note that we have derived Eq. (2) without considering the effect of the boundaries of the acoustic medium. Often it is desirable to calculate the Bragg angle outside of the crystal, $\theta_{B,\mathrm{ext}}$. To close approximation, if the crystal boundaries are parallel to κ, the external Bragg angle is larger than the internal Bragg angle by a factor of n, where n is the refractive index of the acoustic medium.

The cases shown in Figs. 2(a) and 2(b) represent the two geometries where the Bragg matching condition is met for +first-order phonon absorption for a given orientation of κ. Notice that the incident photon wave vector for one case and the diffracted photon wave vector for the other case counterpropagate. This point is relevant to the discussion of the double-pass configuration below. Diagrams similar to those in Fig. 2 can be drawn for the single-phonon emission process, where the diffracted light enters the −first order, and the frequency of the diffracted beam is shifted to $\omega-\Omega$.

B. Acousto-optic devices

A schematic drawing of an acousto-optic modulator is shown in Fig. 3. A rf signal is fed to a strain transducer in contact with the AOM crystal. The rf modulation at frequency Ω causes a traveling density wave to form inside the crystal; the wave propagates at the speed of sound in the crystal, v_s, with the frequency Ω. The refractive index is therefore modulated with a wavelength of $\Lambda=2\pi\cdot v_s/\Omega$, and the crystal acts like a thick diffraction grating with the rulings traveling away from the transducer with a velocity v_s. The Bragg approximation is valid only when the acoustic wave is describable by a plane wave and all phonons have

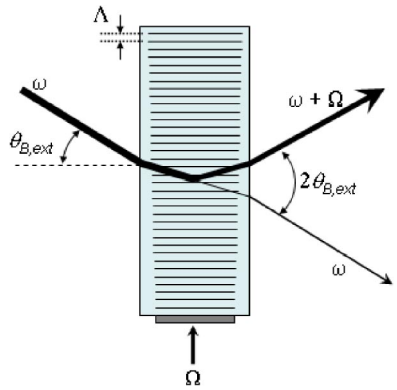

FIG. 3. (Color online) Schematic drawing of an aligned AOM. The AOM is shown in the mode where the light is diffracted into the +first order and the laser frequency is up-shifted by the rf modulation frequency Ω. Note that phonons are absorbed in this configuration, and momentum is transferred to the laser beam in the direction away from the strain transducer. The crystal can also be aligned to be Bragg matched for the −first diffraction order (not shown). In that case, corresponding to a phonon emission process, all of the laser beams are mirror symmetric about the horizontal axis with respect to those shown in the figure, and the diffracted laser frequency is down shifted by Ω. Note that the external Bragg angle is larger than the internal Bragg angle because of refraction at the crystal surfaces.

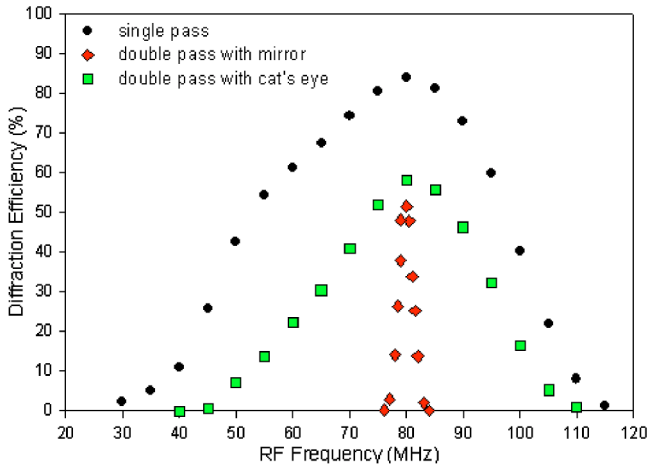

FIG. 4. (Color online) Measured single-pass and double-pass diffraction efficiencies. When comparing the data in the graph, note that for the double-pass measurements the light was diffracted twice by the AOM, and the measurements of the diffracted beam power were performed at the output of a single-mode fiber, which had a coupling efficiency of 80%. It is the overall diffraction efficiency through the fiber that is plotted in the figure for the double-pass data. The double-pass diffraction efficiency at the fiber input is 75%. The double-pass diffraction efficiency measurements were performed with and without the cat's eye lens. Note that since the light frequency is shifted twice for the double-pass measurements, the actual frequency tuning bandwidth is twice the FWHM of the curves. For the double-pass measurements performed with the cat's eye, this corresponds to 68 MHz.

the same wave vector. In practice, this limiting case can be achieved to a close approximation when the strain transducer is long compared to the acoustic wavelength in the direction of laser beam propagation and acoustic diffraction is minimized. It is therefore not uncommon to achieve greater than 80% diffraction efficiency into a single diffraction order with careful engineering.[5] The AOM that we use (Crystal Technology, Inc. 3080-120)[6] has a TeO_2 crystal driven with a longitudinal acoustic mode. At a typical rf frequency of 80 MHz the external Bragg angle is 8 mrad for light with a vacuum wavelength of 852 nm.

C. Bandwidth

The bandwidth is generally defined as the frequency range over which the modulated laser power drops by 50% (3 dB) from the peak value. For the AOM model that we use the specified modulation bandwidth is 20 MHz. The diffraction efficiency that we measured versus rf modulation frequency is presented in Fig. 4 for a single pass through the AOM of a 1.1 mm [full width (FW) $1/e^2$] collimated beam. The full width at half maximum (FWHM) of the curve is ~50 MHz, which is 2.5 times larger than the manufacturer's specified bandwidth. The diffraction efficiencies are the average of four measurements. The values for the absolute errors in the single-pass diffraction efficiency are up to 4%. The double-pass measurements shown in Fig. 4 are discussed in the next section.

IV. DOUBLE-PASS CONFIGURATION

We send light to our apparatus with a number of single-mode optical fibers that facilitate the delivery of laser light to hard-to-reach points on the apparatus and act as spatial filters. While the spatial filtering improves the beam quality and facilitates optics alignment downstream from a fiber, it makes the coupling efficiency for light into the fiber ultrasensitive to the stability of the beam pointing upstream of the fiber. This presents a challenge when the frequency of the light being injected into the fiber is ramped with AOMs, since the Bragg angle depends on the modulation frequency.

The alignment problems caused by AOM frequency sweeps can be practically eliminated by using the double-pass configuration, in which the laser beam travels through the AOM twice and the beam deflection is compensated in the second pass. Modulating the light with the AOM twice also means that the total frequency shift is twice the modulation frequency.

The two momentum conservation diagrams in Figs. 2(a) and 2(b) represent the momentum vectors for the two passes. Notice that the incident and diffracted beams for one case counterpropagate the diffracted and incident beams for the other case. Thus with the alignment optimized, if the +first-order diffracted beam is reflected back onto itself through the AOM for a second pass, the +first-order diffracted beam for the second pass will spatially overlap the original incident beam, independent of the modulation frequency.

Figure 5 is a schematic drawing of our double-pass AOM apparatus, and a photograph is shown in Fig. 6. Light with linear polarization oriented parallel to the page enters the apparatus from the left as shown in Fig. 5. The beam is steered through a polarizing beam splitter and a Galilean telescope by two adjustable mirrors before it enters the AOM. The Galilean telescope reduces the beam diameter from 2.2 to 1.1 mm (FW $1/e^2$) and consists of a plano-convex lens and a plano-concave lens separated by 5 cm. The position of the AOM is constrained by a 3 mm dowel pin, around which the AOM can be rotated about an axis through the center of the crystal. The AOM can be clamped down to the mounting block with two screws after rough

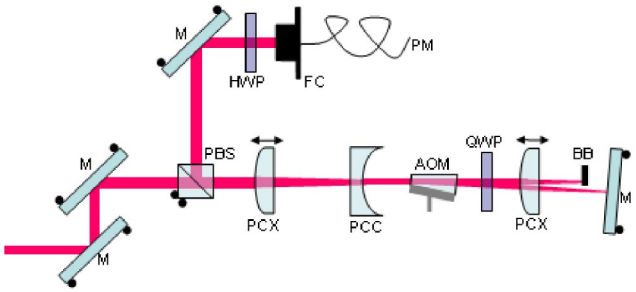

FIG. 5. (Color online) Schematic drawing of the double-pass system. M: mirror; PBS: polarizing beam splitter; PCX: plano-convex lens; PCC: plano-concave lens; AOM: acousto-optic modulator; QWP: quarter-wave plate; BB: beam block; HWP: half wave plate; FC: fiber coupler; PM: polarization maintaining fiber. The circles that are attached to some of the optics represent angular adjustment knobs. The arrows above two of the lenses indicate that they are held in lens-focusing mounts.

angular alignment of the AOM is achieved. Fine angular alignment is accomplished by adjusting the orientation of the two input mirrors. Immediately downstream from the AOM is a quarter-wave plate that circularizes the polarization. The plano-convex lens and mirror downstream from the AOM combine to form the cat's eye retroreflector, which is discussed in detail below. The zeroth-order undiffracted beam is blocked with a beam block before the mirror. The +first-order diffracted beam reflects back from the cat's eye and through the quarter-wave plate, where the polarization is converted back to linear polarization such that the polarization vector is oriented perpendicular to the page on the second pass through the AOM. The light is modulated by the AOM a second time and the resulting +first-order diffracted beam for the second pass overlaps the incident laser beam. The modulated light is then reflected from the adjustable polarizing beam splitter and directed to an adjustable mirror, a half wave plate, and a polarization-maintaining single-mode fiber coupler that contains an 11 mm coupling lens. If beam misalignments of over 1 μm for the focused spot on the fiber core are to be avoided, the angular tolerance for the light beam leaving the AOM is $\sim$0.2 mrad. Note that the Galilean telescope reduces the angular steering of the beam entering the fiber by a factor of 2. Alignment of the laser beam into the fiber coupler is accomplished by adjusting the angles of the mirror and the polarizing beam splitter. To avoid fluctuations of the polarization of the light emerging from the polarization-maintaining fiber, the half wave plate is needed to align the light polarization with the proper axis of the fiber. The base plate to which the optics are mounted is temperature controlled with an inexpensive commercial foil heater and controller. We describe the function of some key features in the apparatus in detail below.

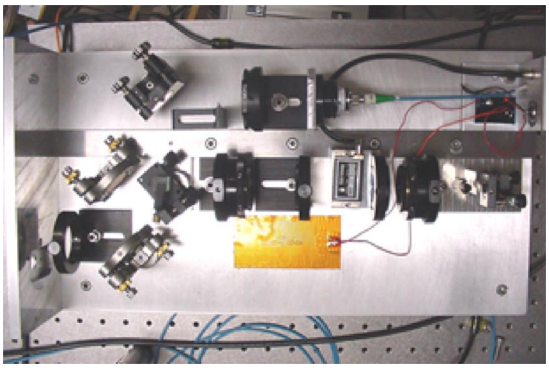

FIG. 6. (Color online) Our double-pass apparatus. The dimensions of the base plate are 25 cm$\times$46 cm.

A. Galilean telescope

The diffraction efficiency for an AOM is a strong function of beam waist diameter, and increases with increasing waist size before leveling off above 90% for a typical diameter of about 0.5 mm. The case enclosing the AOM that we use has laser apertures of 3 mm in diameter, but the active aperture over which the manufacturer guarantees that the device meets specifications is only 1 mm in diameter. The beam size we chose is 1.1 mm (FW $1/e^2$) and is a trade-off between performance and convenience.

The Gaussian beam waist diameter d for a plano-convex lens may be estimated by the formula $d=4\lambda f/\pi D$ in terms of the focal length f, the wavelength λ, and the beam diameter at the lens D. Following the manufacturer's suggestion of using a single plano-convex lens for focusing down the beam while simultaneously optimizing the diffraction efficiency would require the use of a lens with 1 m focal length. If sufficient space is available on the optical table, then we can follow this approach and achieve good diffraction efficiencies with a weakly focused beam.

We can dramatically reduce the size of the apparatus by using a Galilean telescope to reduce the sizes of the laser beams. In principle, by using lenses with very short focal lengths, the length of the telescope can be reduced to a few centimeters. However, there is a trade-off in how small to make the focal lengths. In general, it is much more difficult to fine tune the optical alignment in the apparatus when short focal-length lenses are used to resize the beams. In our apparatus, the input beam has a diameter of 2.2 mm (FW $1/e^2$). We reduce the diameter by a factor of 2 with a +100 mm plano-convex and a -50 mm plano-concave lens spaced by $\sim$50 mm such that the beam entering the AOM is collimated. We mounted the 100 mm converging lens on a commercial lens-focusing mount in order to fine tune the lens spacing. Note that proper orientation of the planar side of the lenses is required to minimize spherical aberrations[4] (see Fig. 5). The alignment of a prototype of the apparatus was much more difficult to optimize and maintain when the Galilean telescope consisted of $f=+50$ mm and $f=-15$ mm lenses.

We also measured the single-pass diffraction efficiency of the AOM with a focused beam by removing the diverging lens, without which the beam waist diameter was $\sim$50 μm in the AOM. If the incident laser beam is strongly focused into the AOM, then there is effectively a range of angles of incidence for the incoming light, and only a fraction of the converging rays are Bragg matched with the crystal. From the point of view of geometric optics, when the beam is focused down, the light rays enter with an angular spread of $\sim$20 mrad. This range is large compared to the external Bragg angle ($\sim$8 mrad), and in this mode only a component of the zeroth-order beam is diffracted into the first-order beam. Since the component of the zeroth-order beam that diffracts depends on the rf frequency, a dark spot is observed

moving across the zeroth-order beam as the rf frequency is swept over the frequency range of the AOM. The maximum diffraction efficiency peaked at approximately 50% of what we observed with a collimated beam.

B. Cat's eye retroreflector

Having a cat's eye[7] as opposed to a simple flat-mirror retroreflector dramatically improves the frequency-tuning range (bandwidth) for the double-pass apparatus. Owing to the dependence of the Bragg angle on the rf modulation frequency, the angle of incidence onto the retroreflector depends on Ω. This can cause the frequency-tuning bandwidth for the double-pass apparatus to be much narrower than for single-pass diffraction, since in practice, the optical alignment is optimized at only a single rf frequency. When the beam arrives at the AOM for its second pass, an imperfect retroreflector causes the angle of incidence on the AOM to deviate from the external Bragg angle and the beam spot position to shift on the AOM. This effect is most problematic when a flat-mirror retroreflector is used.

The standard cat's eye consists of a lens and a mirror with their spacing equal to the focal length of the lens, f. For our application, there is a special configuration for the cat's eye. For optimum performance the spacing between the AOM and the lens should equal the lens focal length.

In this special configuration, as Ω is swept, the diffracted angle is also swept, but when a lens is positioned a distance f from the AOM, the rays emanate from the focal point of the lens, and will emerge from the lens parallel to the zeroth-order beam but deviated by a distance $d = f \cdot \tan(2\theta_{B,\mathrm{ext}})$ for the first-order beam. The angle of the mirror can then be adjusted such that the diffracted beam always hits the mirror at normal incidence independent of the modulation frequency.

The advantage of this special cat's eye configuration was previously noted by Boulanger and co-workers,[8] but they did not present their system in detail and did not inject the modulated light directly into a single-mode fiber. For our apparatus, we find that to efficiently inject the double-passed light into the single-mode fiber without adjusting the beam collimation it is important that the lens-mirror spacing be close to the lens focal length so that the beam is collimated at the single-mode fiber coupler. To be able to optimize the fiber coupling efficiency, we mounted the cat's eye lens onto a commercial lens focusing mount to optimize the lens-mirror spacing. Also, in contrast to what is implied by Boulanger and colleagues, the plano-convex lens in the cat's eye does not have to have a long focal length. We used a lens of half the focal length that they recommended, found the alignment sensitivity unchanged, and still achieved an ideal double-pass bandwidth.

Our cat's eye retroreflector consists of a +75 mm focal-length plano-convex lens and a planar mirror. While the performance is ideal when the AOM-lens spacing is equal to the focal length, the spacing can be reduced by shifting the whole cat's eye toward the AOM to save space if desired without dramatically compromising the bandwidth. For our system, we observe only a 20% decrease in the frequency-tuning bandwidth when the AOM-cat's eye spacing is reduced by 50%.

In principle, we can achieve the same results using a spherical mirror in place of the cat's eye with the mirror positioned at a distance equal to its radius of curvature from the AOM. However, it is difficult to find an inexpensive concave mirror with high reflectivity.

C. Performance

We typically observe diffraction efficiencies exceeding 85% for a single pass and 75% for a double pass. Our data are summarized in Fig. 4, where single-pass and double-pass measurements are presented. It is important to emphasize that, although the three curves are shown together, the values of the diffraction efficiencies for the single-pass and double-pass measurements have different meanings. Whereas the single-pass diffracted power was directly measured at the AOM output, the light for the double-pass measurements was diffracted by the AOM twice and this diffracted light was injected into a single-mode fiber. The power for the double-pass configurations was measured at the fiber output to have a sensitive test on beam pointing stability. The peak double-pass diffraction efficiency is 75% without the fiber, as compared to 85% for the single-pass efficiency, which indicates that the second-pass diffraction through the AOM can be more efficient than the first-pass diffraction.

The ratio of the FWHM for the single-pass measurements to the FWHM of the double-pass measurements performed with the cat's eye is 1.43(7). Assuming a Gaussian dependence, in theory, if there were no beam steering problems, the diffraction efficiency function for the single-pass should be squared to arrive at the diffraction efficiency frequency dependence for the double pass. Thus, the optimum ratio of the single-pass to the double-pass bandwidth is $\sqrt{2}$, in agreement with what we observe. This agreement shows that the cat's eye acts as an ideal retroreflector. Note that the frequency dependencies shown in Fig. 4 are in terms of the rf modulation frequency, not the actual frequency shift, which is two times larger for a double pass. So, in terms of the frequency tuning range, the bandwidth of the double pass with the cat's eye is larger than that of the single pass by $\sqrt{2}$.

Quite striking is the difference between the double-pass measurements performed with and without the cat's eye lens. Having the cat's eye retroreflector as opposed to a planar mirror increases the frequency-tuning bandwidth of the device by about one order of magnitude.

ACKNOWLEDGMENTS

The authors thank M. A. Lombardi and D. R. Smith for helpful comments on this manuscript. This work is a contribution of NIST, an agency of the U.S. government, and is not subject to copyright.

[1] C. Solomon, J. Dalibard, W. D. Phillips, A. Clairon, and S. Guellati, Europhys. Lett. **12**, 683 (1990).
[2] C. G. Townsend *et al.*, Phys. Rev. A **52**, 1423 (1995).
[3] S. R. Jefferts *et al.*, Metrologia **39**, 321 (2002).
[4] R. Guenther, *Modern Optics* (Wiley, NewYork, 1990).
[5] E. H. Young and S. Yao, Proc. IEEE **69**, 54 (1981).

[6] Products or companies named here are cited only in the interest of complete scientific description, and neither constitute nor imply endorsement by NIST or by the US government. Other products may be found to serve just as well.

[7] J. J. Snyder, Appl. Opt. **14**, 1825 (1975).

[8] J. S. Boulanger, M. C. Gagné, and R. J. Douglas., Proceedings of the 11th European Frequency and Time Forum, Neuchatel, France, 4–6, March, 1997, pp. 567–571.